JOURNAL OF MATERIALS SCIENCE **36** (2001) 3011 – 3025

Fracture variability and R-curve behavior in yttria-stabilized zirconia ceramics

D. CASELLAS, J. ALCALÁ, L. LLANES, M. ANGLADA
Departament de Ciència dels Materials i Eng. Metal.lúrgica, Universitat Politècnica de Catalunya, E.T.S. d'Enginyeria Industrial, 08028 Barcelona, Spain
E-mail: alcala@cmem.upc.es

An assessment of fracture origins is conducted in yttria-stabilized zirconia ceramics containing different grain sizes. As the microstructure coarsens due to the application of heat treatments, fracture origins change from single pores to transformed regions at the free surface which are induced by the applied stress. The observation of an increasing size of failure origins with microstructural coarsening lies as the underlying reason for the finding that specimens containing coarser microstructures and a more pronounced R-curve behavior do not fail at larger stresses. A fracture model is used to link the strength variability of a fully tetragonal zirconia containing a small grain size to its pore size distribution. The increased transformability of zirconia ceramics with coarser tetragonal grains is evaluated by means of quantitative phase analysis, characterizations of fracture surface morphology, and R-curve assessments. It is confirmed that tetragonal grains of up to 4 μm may not necessarily undergo a spontaneous t–m transformation upon cooling from sintering.

1. Introduction

The understanding of the fracture behavior of ceramic materials has been the focus of intensive research for more than 30 years. Fracture assessments in ceramics are usually conducted considering either their strength variability via Weibull statistics or their R-curve behavior. While the former is usually regarded as an approach to structural design with brittle materials, the R-curve allows to develop a fundamental comprehension of fracture micromechanisms.

The R-curve provides a tool for the evaluation of the crack growth resistance of ceramics using concepts from fracture mechanics. This curve is presented as a plot of the applied stress intensity factor in terms of crack growth. A rising R-curve behavior is indicative of the development of toughening mechanisms, such as the tetragonal-to-monoclinic (t–m) phase transformation in zirconia and crack-bridging, which "shield" the crack tip from the applied loads [1]. Thus, in the case of monolithic zirconia ceramics, a rising R-curve can be promoted by increasing the transformability of small tetragonal particles. This can be achieved, for example, by coarsening the grain size of the material by recourse to suitable heat treatments.

A direct result of a rising R-curve behavior is the attainment of *stable* crack growth over a range of the applied stress intensity factor for which unstable fracture would have been triggered in the absence of toughening mechanisms. Accordingly, a rising R-curve behavior would be anticipated to induce an increase in fracture strength. However, such concomitant increase of the crack growth resistance and fracture strength is seldom confirmed by experimental measurements in ceramic materials. In this sense, a general trend found in brittle materials is that the fracture strength under monotonic loads increases as the grain size decreases [2]. For example, yttria-stabilized tetragonal zirconia polycrystals (Y-TZP) whose grain size lies in the submicron range fails at ~1000 MPa, while magnesia partially-stabilized zirconias (Mg-PSZ) whose grain size is in the 50-μm range fail at ~500 MPa. The general explanation accounting for these observations is that ceramics with small grain sizes contain smaller flaws than materials with large grain sizes. An interesting aspect in the above comparison is that the fracture strength of Mg-PSZs is much lower than that of Y-TZPs even when the former possess a larger crack growth resistance [3, 4].

The present work was conducted with the general objective of assessing the interplay between fracture strength, R-curve behavior and failure origins in yttria-stabilized zirconia ceramics. The systematic evaluation of fracture strength variability and failure origins in Y-TZP materials with different grain sizes (resulting from the application of a heat treatment) is expected to shed light into the underlying reasons why ceramic materials which display a more pronounced R-curve behavior have the tendency to fail at lower stresses. A quantification of the influence of flaw population and R-curve on the fracture strength variability in a fine grained Y-TZP is also attempted in this work. Such rationalization is important in bridging the gap between statistical concepts used in structural design with ceramics and more fundamental issues involving their crack growth (R-curve) behavior.

An evaluation of the increased transformability of Y-TZP as the grain size coarsens is also conducted in this work by means of crack growth assessments and in-depth microstructural characterizations. Such evaluations are significant in light of recent investigations where the heat treatment of a Y-TZP at elevated temperatures was found to produce tetragonal grains with a size of up to 5 μm which do not transform spontaneously to the stable monoclinic structure upon cooling to room temperature [5]. This observation is potentially relevant as it may lead to the processing of zirconias with an enhanced capacity for undergoing a stress-assisted t–m transformation, with the consequent increase in crack growth resistance.

2. Materials and experimental results

2.1. Materials

The starting material was a fully tetragonal 2.5 mol% Y-TZP containing 1 mol% HfO_2. This material had a grain size of $\sim$0.3 μm, Fig. 1a. Such fully tetragonal structure results from sintering within the tetragonal field of the ZrO_2–Y_2O_3 phase diagram. Further heat treatment at 1650°C for 2 and 10 hours places the material within the tetragonal + cubic field of the phase diagram, inducing the nucleation of large cubic grains of $\sim$5 μm and coarsening of the small tetragonal grains in a similar manner as described in Ref. [5] (Fig. 1b and c). The heat treatment of the material for 2 hours at 1650°C coarsens the *mean* tetragonal grain size to $\sim$1.4 μm, whereas an increase in heat-treating time to 10 hours induces the coarsening of such grains to a mean size of $\sim$2.3 μm (see Table I). As large cubic grains were also induced upon heat treatment at 1650°C, the resulting materials had a combined Y-TZP/PSZ character. (According to the nomenclature commonly used when referring to zirconia ceramics, partially stabilized zirconias (PSZ) contain large cubic grains whereas TZP materials are formed exclusively by small tetragonal particles. PSZ microstructures also contain tetragonal precipitates within the cubic grains. As noted in the foregoing discussion, such small precipitates were also detected in the heat-treated Y-TZP/PSZ materials.) The residual porosity content in all materials was $\sim$2%.

X-ray diffraction and Raman microprobe spectroscopy were used to perform a quantitative analysis of the phases present in flat surfaces of the as-sintered and heat-treated materials when polished to a 0.3–μm finish. These techniques were also applied

TABLE I Microstructructual features

Material	Volume fraction of cubic grains	Volume fraction of tetragonal phase	Volume fraction of monoclinic phase at fracture surface	Grain size[§], d (μm)
Y-TZP (as-sintered)	0	1.00	0.05 ± 0.03	0.3
Y-TZP/PSZ (heat-treated for 2 hours)	0.23 ± 0.03	0.77	0.32 ± 0.06	1.4
Y-TZP/PSZ (heat-treated for 10 hours)	0.37 ± 004	0.63	0.39 ± 0.04	2.3

[§]For tetragonal grains.

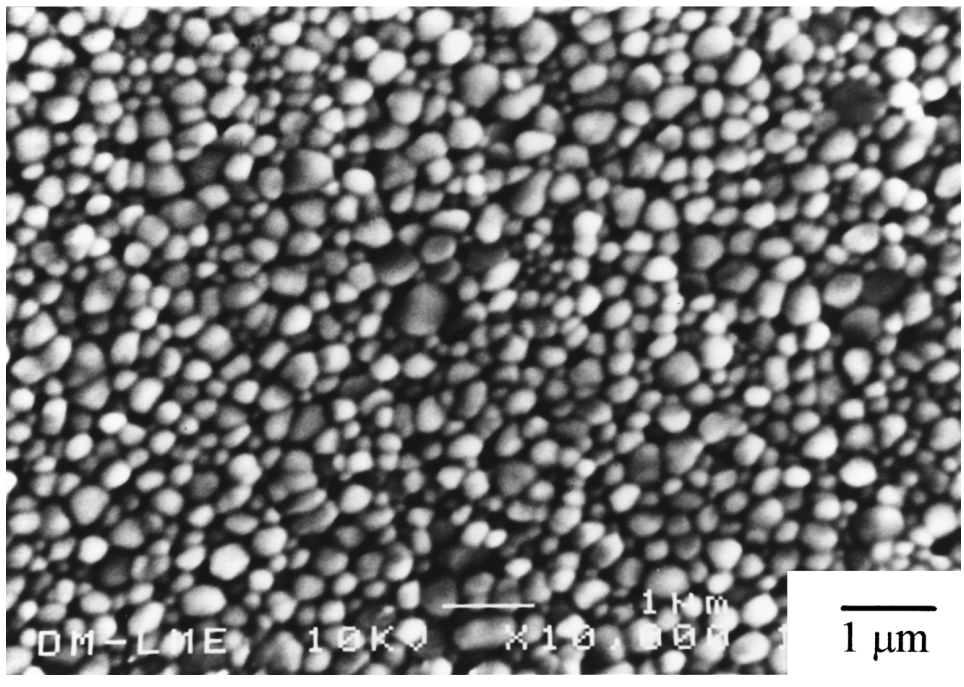

(a)

Figure 1 Microstructure of the materials. (a) as-sintered state, (b) heat-treated for 2 hours, (c) heat-treated for 10 hours. Note the increase in the size of the tetragonal (t) grains as heat-treating time increases. *(Continued.)*

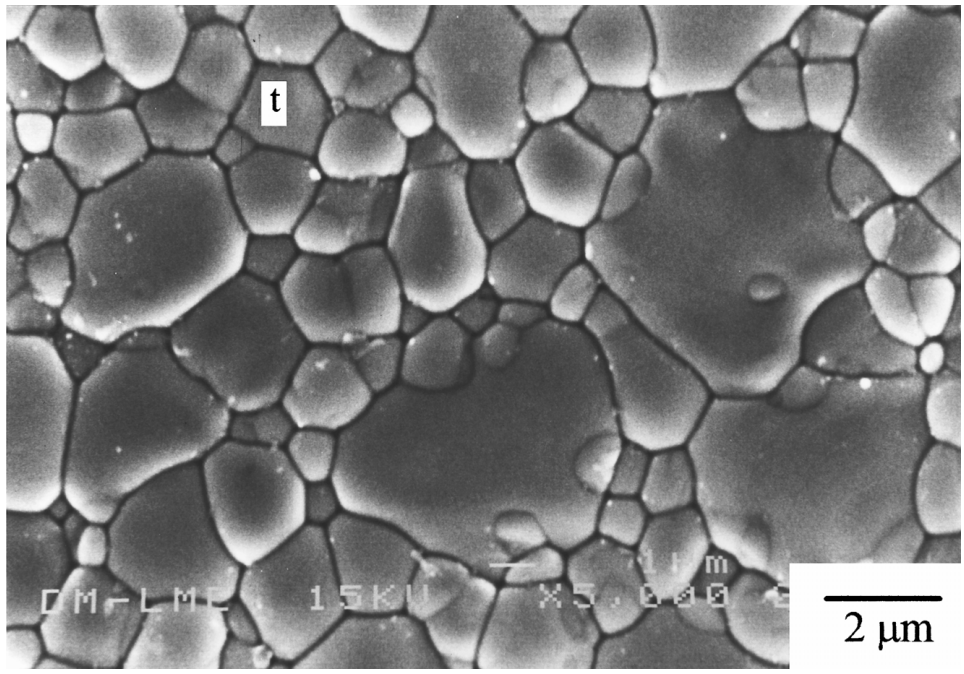

(b)

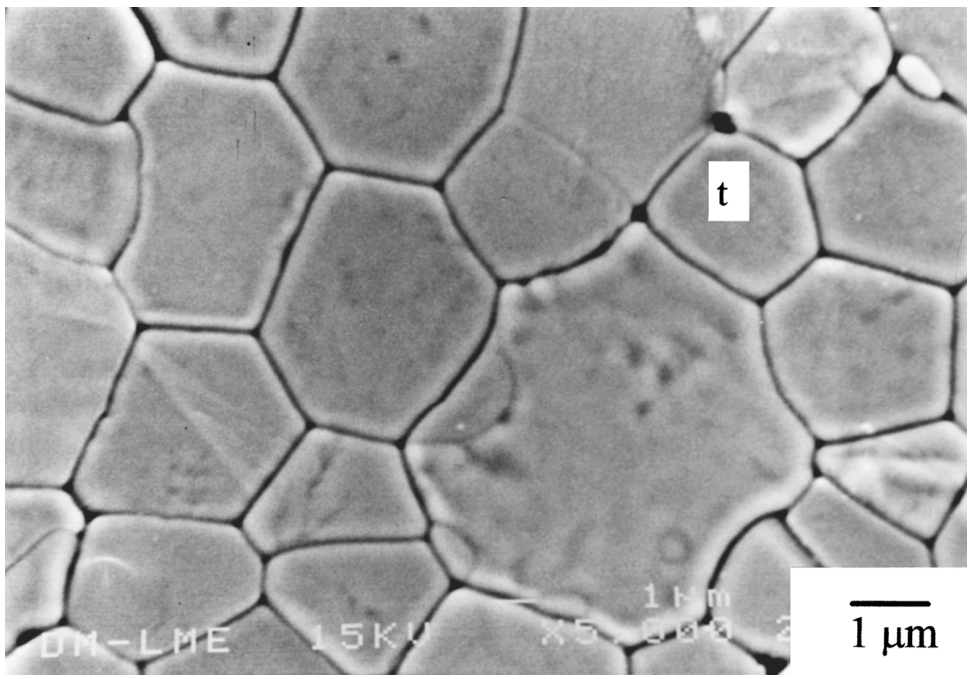

(c)

Figure 1 (Continued.)

to the fracture surfaces of all materials. The fraction of tetragonal, monoclinic and cubic phases were measured using X-ray diffraction where Cu Kα radiation with wavelength, λ, = 0.1548 nm was used (see Ref. [6] for details). An important feature of Raman spectroscopy was its capability of evaluating phase contents within a small region of the sample [7]. Such measurements were conducted with a HeNe laser with $\lambda = 633$ nm. The fraction of cubic and tetragonal phases present in the materials is reported in Table I, along with the monoclinic fraction detected at the fracture surfaces which is the consequence of the stress-assisted t–m transformation.

The increased capacity of the studied materials to experience t–m transformation as the tetragonal grain size coarsens is evident from Table I. This table shows that the monoclinic phase at fracture surfaces increases gradually from ~5% in the as-sintered Y-TZP to ~40% for the heat-treated Y-TZP/PSZs. It is noted that even when the size of individual tetragonal grains increased to ~3.7 μm upon heat treatment, spontaneous transformation to the monoclinic (stable) structure upon cooling did not occur. This confirms the results in Ref. [5] which show that the critical tetragonal grain size for spontaneous transformation at room temperature in Y-TZP may be much larger than 1 μm.

Raman spectroscopy showed that in the Y-TZP/PSZs, most of the tetragonal grains around indentation-induced cracks (see Fig. 2) underwent a stress assisted

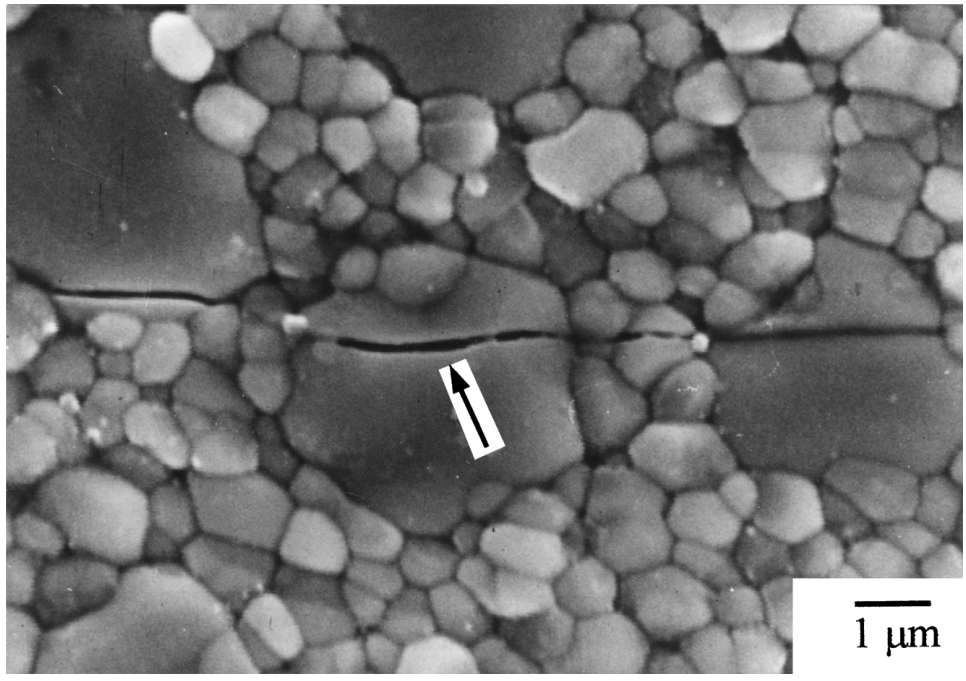

Figure 2 Surface profile of an indentation induced crack in a heat-treated material. Arrow shows the transgranular fracture at cubic grains.

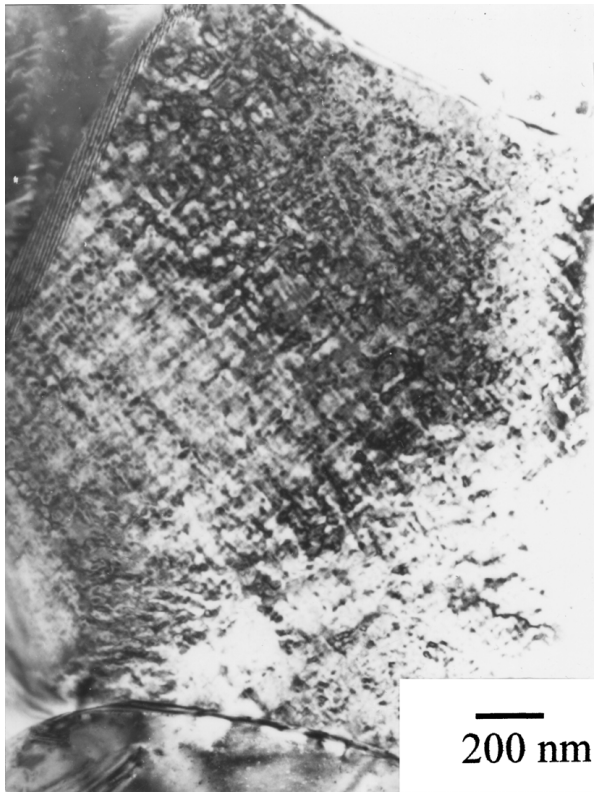

Figure 3 Rumpling at a cubic grain induced by small tetragonal precipitates.

t–m transformation. An interesting result, as evidenced by transmission electron microscopy (TEM), was that the cubic grains in Y-TZP/PSZ materials contained tetragonal precipitates of a very small size (Fig. 3). However, Raman spectroscopy around the indentation cracks showed that the tetragonal precipitates within cubic grains did not experience t–m transformation, probably as a result of their minute size which tends to stabilize the tetragonal structure. Thus, the increased capacity of the heat-treated materials to undergo transformation toughening mechanisms is due only to the t–m transformation of the tetragonal grains and not of the tetragonal precipitates dispersed within the cubic grains.

2.2. R-curve assessments

The R-curve of the materials was evaluated using semielliptical surface cracks which were loaded under four-point bending. The precracking procedure used as well as the R-curve results are described in this section. First, Vickers indentations were placed in the prospective side of square bars to be subjected to tensile stresses. The resulting indentation cracks were aligned parallel to the thickness of the specimens. In all materials the cracks had a radial geometry as described in Refs. [8, 9]. In accord with the findings in Ref [10], heat treatment at 1100°C for 1 hour of the as-sintered material induced the growth of indentation cracks so that their geometry evolved from a radial to a half-penny configuration. Microstructural changes were not induced by such heat treatment. Upon heat treatment of the the specimens at 1100°C, the indented surface was ground to remove the inelastic zone (ligament) underneath the indent as such ligament is known to affect crack growth under external loads (see Ref. [10]). It is noted that the application of the above procedure led to surface cracks which are free of any indentation precracking effects.

In the case of the Y-TZP/PSZ materials, the resulting indentation cracks were shallower than in the as-sintered Y-TZP. Thus, surface grinding led to the removal of both the ligament underneath the imprint as well as the cracks. For this reason, Y-TZP/PSZ specimens were tilted by ∼3–5° out of the plane normal to the indentation loading axis so that preferential growth of the cracks in one direction was promoted during

indentation precracking [11]. The application of this technique induced cracks with different lengths in opposite corners of the imprint. Care was exercised to align the larger crack along the thickness of the specimen. Subsequently, surface grinding was carried out to fully remove the shorter cracks and the constraining ligament while a single crack suitable for loading under pure mode I was left at the surface.

All specimens were heat-treated at 1200°C for 10 minutes prior to testing under four-point bending. This fully reverted the t–m transformation around the cracks which was induced by indentation precracking, removing crack loading history effects. As confirmed by X-ray diffraction, such heat treatment did not produce further microstructural changes.

R-curve assessments were conducted using the so-called "dummy indentation technique" [12]. Such testing procedure requires that several indents are placed at the surface of the specimen where the tensile stress is constant under four-point bending (i.e., within the inner span of the loading fixture). The specimen is then fractured and the maximum load recorded. This measurement is used in conjunction with the length of surviving indentation cracks to compute the applied stress intensity factors in each of the cracks. Finally, a plot of the applied stress intensity factor, K, in terms of crack growth provides the R-curve of the material.

Square bars of $5 \times 5 \times 45\ \text{mm}^3$ were used in the measurement of the R-curve. The load was applied at a rate of 200 N/s using a screw-driven mechanical testing machine. A self-aligning four-point bending fixture having inner and outer spans of 20 and 40 mm, respectively, was used in the experiments. The length of surviving cracks was measured by optical microscopy with a resolution of $\pm 1\ \mu$m. The ellipticity of the cracks used in the computation of K was evaluated from fracture surface observations [10]. The formulation of the stress intensity factor for semi-elliptical cracks derived in Ref. [13] was used in the calculation of the crack growth resistance, K_r, for each of the cracks.

TABLE II R-curve parameters

Material	K_o (MPa$\sqrt{}$m)	K_m (MPa$\sqrt{}$m)	δ (μm)
Y-TZP (as-sintered)	3.9	0.3	29
Y-TZP/PSZ (heat-treated for 2 hours)	5.0	1.6	19
Y-TZP/PSZ (heat-treated for 10 hours)	5.8	2.3	29

Fig. 4 shows the R-curves measured in all materials. Zirconia ceramics subjected to the heat treatment to coarsen their microstructure achieved the maximum crack growth resistance. This is in agreement with the improved capacity of the Y-TZP/PSZ materials to undergo t–m transformation, Table I. The results of the parameterization of the R-curve according to [14]

$$K_r = K_o + K_m \operatorname{arctg}\left(\frac{\Delta c}{\delta}\right) \tag{1}$$

are presented in Table II. In Equation (1), the factor K_o is introduced to account for the intrinsic fracture resistance, K_r, of the material prior to crack growth; K_m and δ are material constants; and Δc is the growth of the cracks in the radial direction as measured from their center.

Evidence of t–m transformation as the active toughening mechanism of the materials is provided in Fig. 5, where the size of the transformation zone around indentation cracks is clearly detected.

2.3. Fracture strength measurements

Cylindrical bars of 8 mm in diameter were loaded under three-point bending with a total span of 40 mm to obtain accurate measurements of the fracture strength distributions. The load was applied at a rate of 200 N/s, and the maximum (fracture) load recorded. A total of 60 tests were conducted with each of the materials.

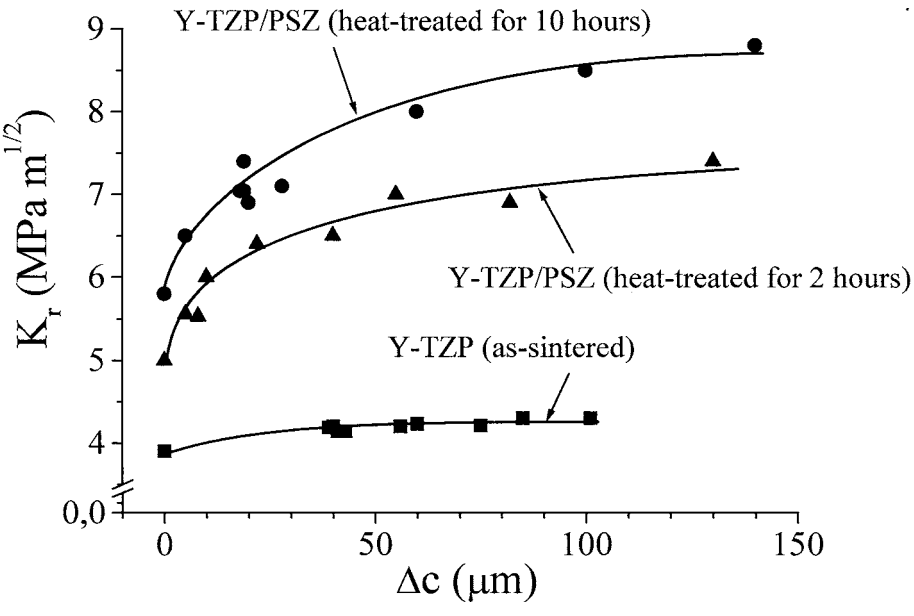

Figure 4 R-curves for the as-sintered and heat-treated materials.

Prior to testing, all specimens were polished with diamond paste to a 0.3-μm finish to reduce the influence of machine damage on strength distributions. The fact that the cylindrical specimens do not contain sharp edges as in the case of square bars is beneficial in ensuring that the fracture response is a unique consequence of the flaw population within the specimens.

The loading rate applied is assumed to be sufficiently high as to disregard the influence of environmentally-assisted stable crack growth in the strength distributions. Fracture experiments conducted at a loading rate two orders of magnitude lower ($\sim$2 N/s) evidenced a decrease of the mean fracture strength of only $\sim$10–15%. This is a minute difference considering that fracture occurred after $\sim$ 40 min of loading, instead of the usual 20 s for a loading rate of 200 N/s.

The failure probability, P_f, for every specimen was computed by ranking the results of fracture strength in ascending order using the relation

$$P_f = \frac{n}{N+1}, \tag{2}$$

where n is the number of specimens failing below a given bending stress, and N is the total number of specimens used in the fracture experiments.

The fracture distributions were assumed to follow Weibull statistics according to

$$P = 1 - \exp\left[-\left(\frac{\sigma_\mathrm{f}}{\sigma_\mathrm{o}}\right)^m\right], \tag{3}$$

where σ_f is the fracture stress of the outer fiber in the three-point bending bar, and $\sigma_\circ$ and m are material constants which govern the fracture stress distribution. The values of m and $\sigma_\circ$ for present materials are found from a linear fit to a plot of ln (ln(1 / (1$-P_f$)) in terms of ln σ_f (where such linear fit becomes evident by solving Equation (3) for (1 $- P_f$) and taking logarithms), see Fig. 6 and Table III. It is noticed that m increases slightly for the Y-TZP/PSZ materials, in agreement with the general conception that the development of a rising R-curve brings about a narrowing in the fracture strength statistics.

TABLE III Weibull parameters

Material	σ_o (MPa)	m
Y-TZP (as-sintered)	1116	14.0
Y-TZP/PSZ (heat-treated for 2 hours)	1058	15.5
Y-TZP/PSZ (heat-treated for 10 hours)	938	17.4

2.4. Fracture surface morphology

The fracture surfaces of the material in the as-sintered state had a mixed inter- trans-granular character, Fig. 7a. Fracture surface observations in the Y-TZP/PSZ materials evidenced an increased tendency of the tetragonal grains to fracture in a transgranular manner as their size coarsened with heat-treating time (Fig. 7b and c). Tetragonal grains fracturing transgranularly in the Y-TZP/PSZ materials had a rough appearance which contrasts with the "clean" transgranular failure of cubic grains (Figs 2 and 8a). Detailed scanning electron microscopy (SEM) observations showed that the rough transgranular fracture of tetragonal grains was associated with the formation of thin strips (bands) which spreaded across the grains, Fig. 8a. These bands seem to be originated by transformation twins which were clearly evidenced by TEM observations in such large tetragonal grains, Fig. 8b. The fact that an increased fraction of monoclinic phase was detected at the fracture surfaces of Y-TZP/PSZ materials (containing the largest and thus, less stable tetragonal grains) agrees well with the consideration that the

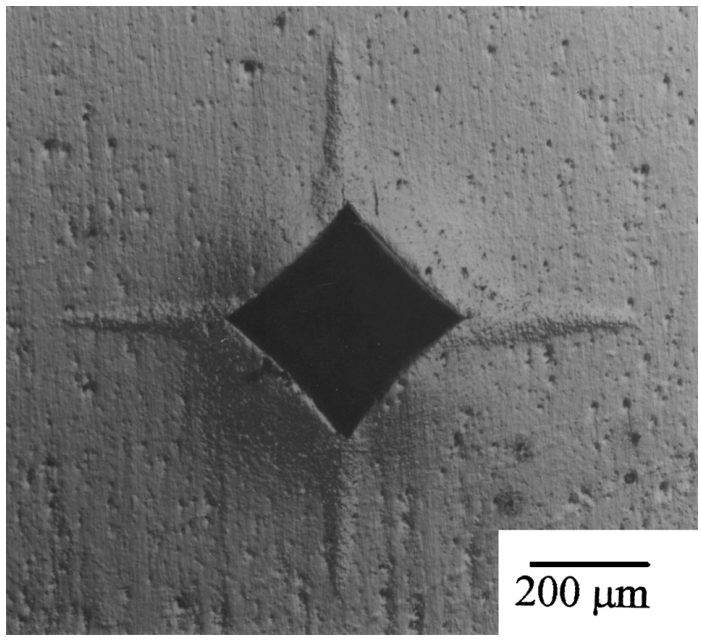

Figure 5 t–m transformation surrounding a Vickers indent induced with an indentation load of $\sim$600 N in a Y-TZP/PSZ material.

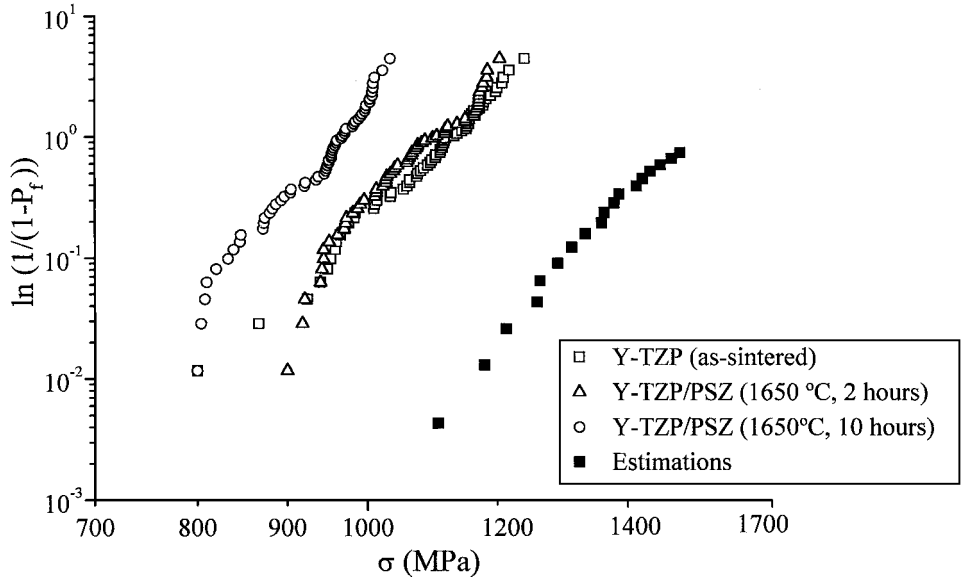

Figure 6 Weibull plots for the zirconia ceramics.

aforementioned bands in tetragonal grains are due to t–m transformation.

The above results for the Y-TZP/PSZ materials contrast with fracture surface assessments conducted in the as-sintered state, where the occurrence of transgranular fracture in tetragonal grains *cannot* be associated with their t–m transformation. In this case, only 5% of the tetragonal grains transform to the monoclinic structure despite the percentage of transgranular features could reach more than 50% of the total fracture surface.

Present results suggest the existence of a critical tetragonal grain size above which transgranular fracture leads to t–m transformation. For small grain sizes the stability of the tetragonal phase is large and t–m transformation may not be attained even when fracture may be predominantly transgranular. As the tetragonal grain size coarsens, transgranular fracture of such grains inevitably results in t–m transformation. The high-temperature crack growth results in Ref. 16 indicate that the grain boundary character (e.g. presence of glassy phases) ultimately controls the fracture morphology in Y-TZP. This reference shows that grain boundary decohesion is promoted as temperature increases, shifting the room temperature transgranular fracture of a small-grained Y-TZP to a fully intergranular fracture character at elevated temperatures.

3. Discussion

3.1. Fracture origins and their influence on fracture strength

Over 40 fracture surfaces from bending tests were examined by SEM to perform a detailed assessment of crack-initiating sites in the materials under study. Fig. 9a and b shows that in the as-sintered state, fracture originates from pores which are located at the specimen surface, close to the point of maximum bending stress. From the ~15 fracture surfaces examined for specimens in the as-sintered condition, only in one case failure was triggered by a large (sintering) agglomerate located away from the specimen surface. These results are consistent with prior observations which indicate that the pores constitute important failure origins in Y-TZP [15]. Such crack-initiating pores are remnant from sintering and their size ranges from 8–15 μm. Experimental measurements of the size of the pores were carried out by SEM observations of polished samples. Fig. 10 presents the size distribution of such pores for the as-sintered Y-TZP as measured in a total cross-sectional area of ~200 mm^2 which encompass 5 different specimens (in this figure, $g(R)$ gives the probability that a given pore size is present in a unit volume of material in accordance with the derivations presented in the Appendix). A similar pore size distribution was found for the Y-TZP/PSZ materials.

The SEM observations at the fracture surfaces of the as-sintered Y-TZP showed the presence of regions of "white-contrast" surrounding the pores, where fracture was predominantly *intergranular* (see Fig. 9b). The relevance of these regions to the fracture process of the material is considered next. The intergranular fracture morphology may indicate the existence of mechanically weak areas, where microcracks nucleate under external loads. On the other hand, such intergranular fracture features may be induced by crack nucleation events around pores upon cooling from sintering temperature. In this regard, complementary observations of fracture surfaces originated by indentation crack growth at high temperatures confirmed that the as-sintered material displayed fully intergranular fracture features (such transition towards a fully intergranular morphology at high temperatures from the mixed inter-trans- granular mode taking place at room temperature is identical to that previously reported in the Y-TZP in Ref. [16].) These results may suggest that, upon cooling from processing, small cracks may nucleate around the pores by thermal expansion mismatch between neighboring grains. This consideration is in good accord with the stress concentration effects which are induced around free surfaces such as pores due to thermal mismatch [18]. The cracks nucleated under such

thermo-mechanical loading would then grow in fracture experiments conducted at room temperature.

It is important to note that direct experimental results on crack nucleation events around pores are scarce and that, to the present, it is not possible to substantiate a crack nucleation sequence in ceramics. Prior work indicates that acoustic emission marks the initiation of fracture events in alumina when loaded at ∼50% of the fracture strength [17]. It is not possible, however, to conclude whether these events are due to the *nucleation* of microcracks around defects such as pores, or if acoustic emission is a manifestation of the growth of *pre-existing* cracks.

In the Y-TZP/PSZ materials, failure was not triggered by a single pore but by larger regions located at the *surface* of the specimen containing several pores. Fracture was predominantly intergranular around such failure origins and their length was ∼40 μm, Fig. 11a and b. Such length is in agreement with the radius of an equivalent circumferential crack which would trigger failure at the mean value of the fracture stress distribution if the crack growth resistance was taken as the maximum fracture toughness of the R-curve (∼7 MPa$\sqrt{\text{m}}$). Raman spectroscopy measurements conducted in the polished (free) surface of the specimen at the precise location where fracture was initiated showed the presence

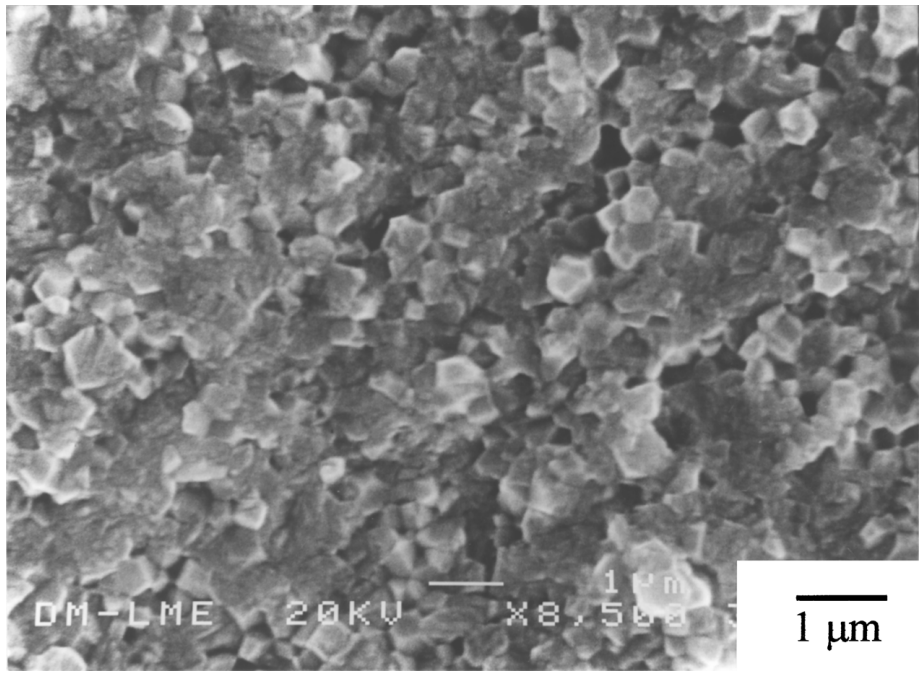

(a)

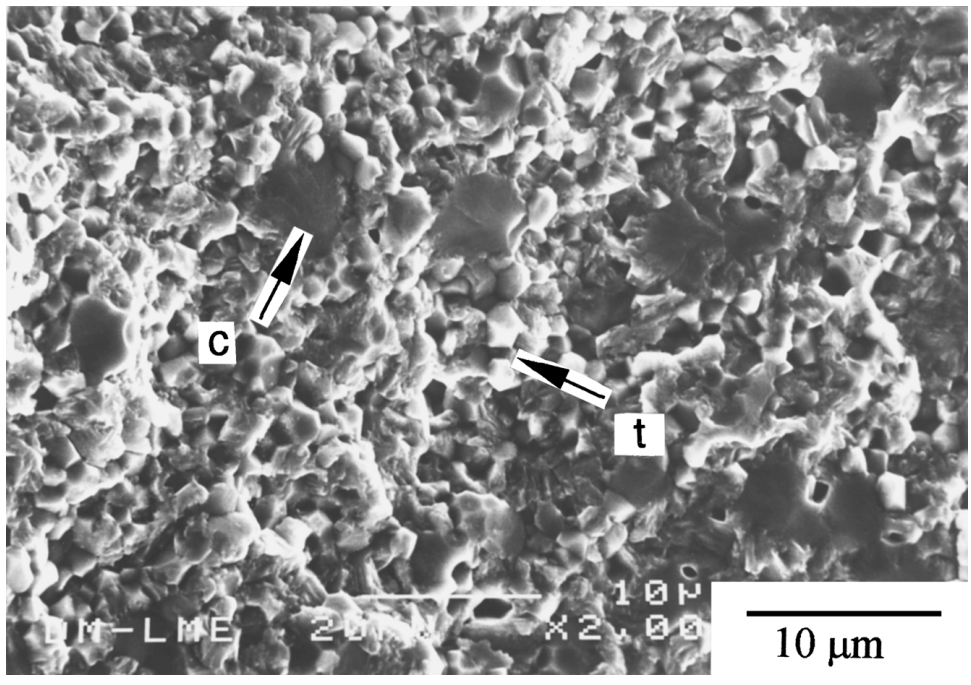

(b)

Figure 7 Fracture surface morphologies. (a) as-sintered Y-TZP, (b) Y-TZP/PSZ heat-treated for 2 hours, (c) Y-TZP/PSZ heat-treated for 10 hours. Arrows indicate tetragonal (t) and cubic (c) grains *(Continued.)*

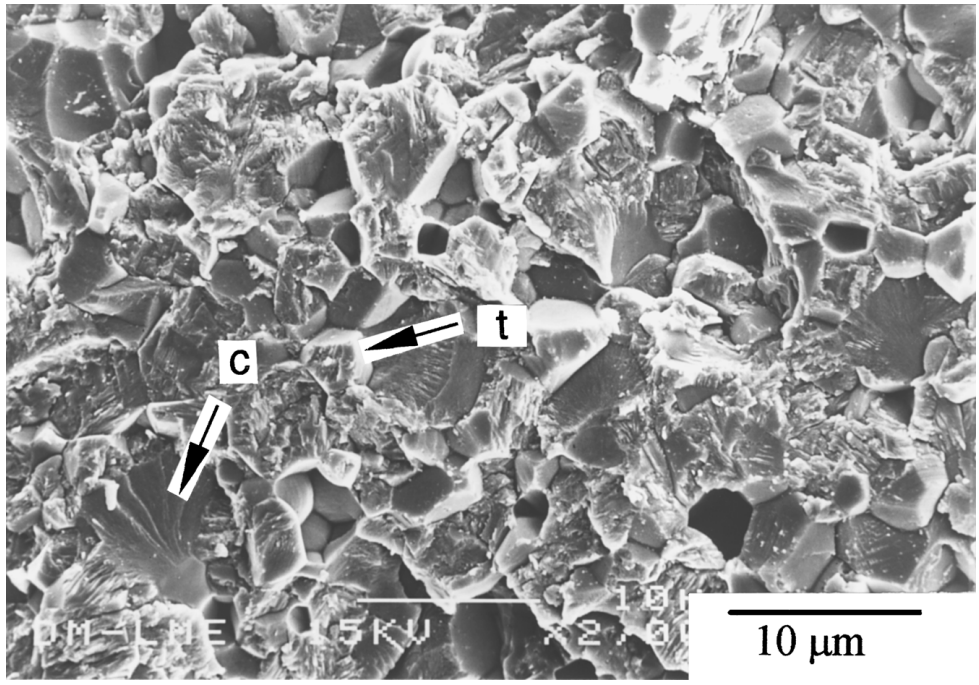

(c)

Figure 7 (Continued).

of a significant amount of monoclinic phase. Such large monoclinic phase content was not detected by any other measurements encompassing larger regions throughout the free surface of the specimen.

Present findings indicate that failure micromechanisms in the Y-TZP/PSZ materials are distinctly different to those in the as-sintered Y-TZP. In the Y-TZP/PSZ ceramics, failure seems to be initiated by stress induced t–m transformation at the free surface which then leads to microcrack formation and coalescence. Such microcrack coalescence produces the large failure origins observed by SEM. The postulated fracture process for the Y-TZP/PSZ materials contrasts with that taking place in the as-sintered Y-TZP, where failure is the result of crack propagation around a single pore.

It is usually considered that the size of failure origins and the rising R-curve behavior which results from the development of toughening mechanisms dictate the fracture strength distributions in ceramics. Upon the development of toughening mechanisms, the unstable growth of pre-existing defects is shifted to larger values of the applied K, thus increasing the fracture resistance of the material. Present results seem to indicate that as the size of failure origins *increases* with the advent of transformation toughening mechanisms in the Y-TZP/PSZ materials, the fracture strength may undergo a modest decrease with heat-treating time, Fig. 6.

While the above interplay between the R-curve and the size of failure origins may well explain the fact that fracture stresses have a certain tendency to decrease upon the development of toughening mechanisms, alternative fracture mechanisms can be postulated to account for such strength reduction. In this regard, it is noted that clusters of cubic grains were also identified as failure origins in the Y-TZP/PSZs, Fig. 11c. The size of these clusters ($\sim$30 μm) was also much larger than the size of the crack-nucleating pores ($\sim$10 μm) in the as-sintered Y-TZP specimens.

3.2. Fracture model

The fracture stress distribution of the as-sintered Y-TZP is studied in this section by recourse to a simplified fracture model. Such fracture model is advocated as a tool for the prediction of the stress distribution in polycrystalline materials where the fracture process involves crack nucleation and growth around a single pore. The development of a fracture model for the Y-TZP/PSZ materials is not attempted here as it would inevitably require the consideration of more complicated failure micromechanisms involving t–m transformation and microcrack coalescence around multiple pores.

The following are the assumptions made in the formulation of the model:

- Circumferential cracks originate from pores and their propagation under external loads controls the fracture strength of the material [19]. Directing attention to Fig. 12, the initial crack length, c, is assumed to remain constant throughout the entire pore population. Such crack length is an important variable as, upon load application, it sets the value of the applied stress intensity factor around each pore.
- The tangency between the R-curve and the applied stress intensity factor defines the stress level and crack extension triggering unstable fracture [1]. Thus, unstable fracture will occur when the applied stress intensity factor (K_a) is larger than the R-curve (K_r). Various studies are available on the stress intensity factor for a circumferential crack emanating from an embedded spherical pore

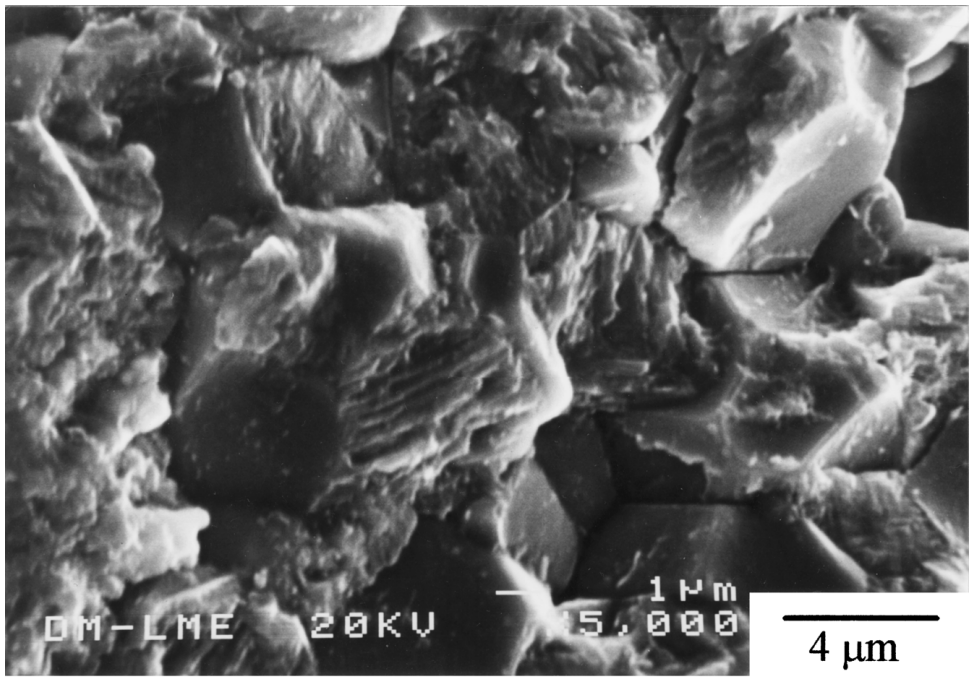

(a)

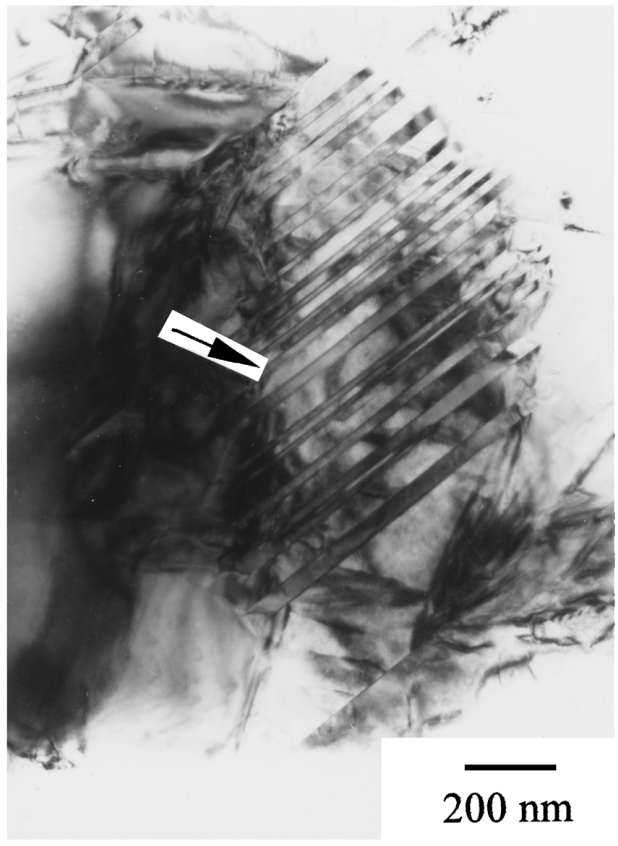

(b)

Figure 8 (a) Detail of the bands present in tetragonal grains fracturing transgranularly; (b) t–m transformation twins as evidenced by TEM (see arrow).

[17, 19, 20]. For simplicity, the relation between the "normalized stress intensity factor" and c/R in Fig. 4 of Ref. [17] is fitted to the following equation

$$K_a = f(c/R)\,\sigma_f\sqrt{\pi c}, \quad f(c/R) = \frac{b + s \times (c/R)}{1 + q \times (c/R)} \tag{4}$$

where σ_f is the fracture stress, $b = 2.51$, $s = 2.34$ and $q = 3.87$.

- It is assumed that strength-controlling cracks emerge from pores prior to the application of loads. It is also considered that a transformation zone is not present around such cracks as it develops gradually during crack growth under the applied loads.

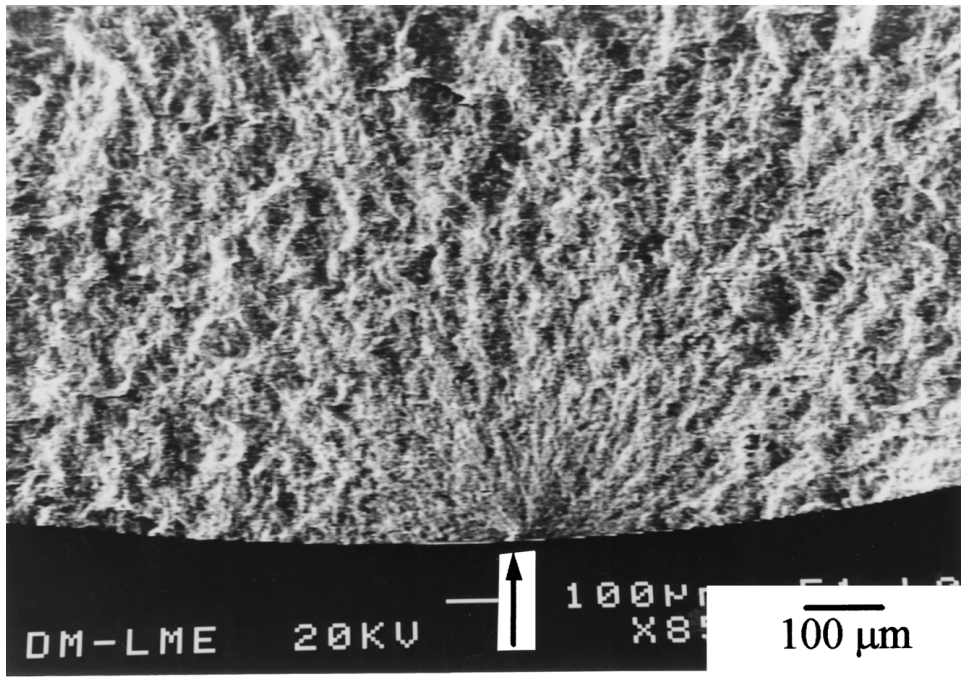

(a)

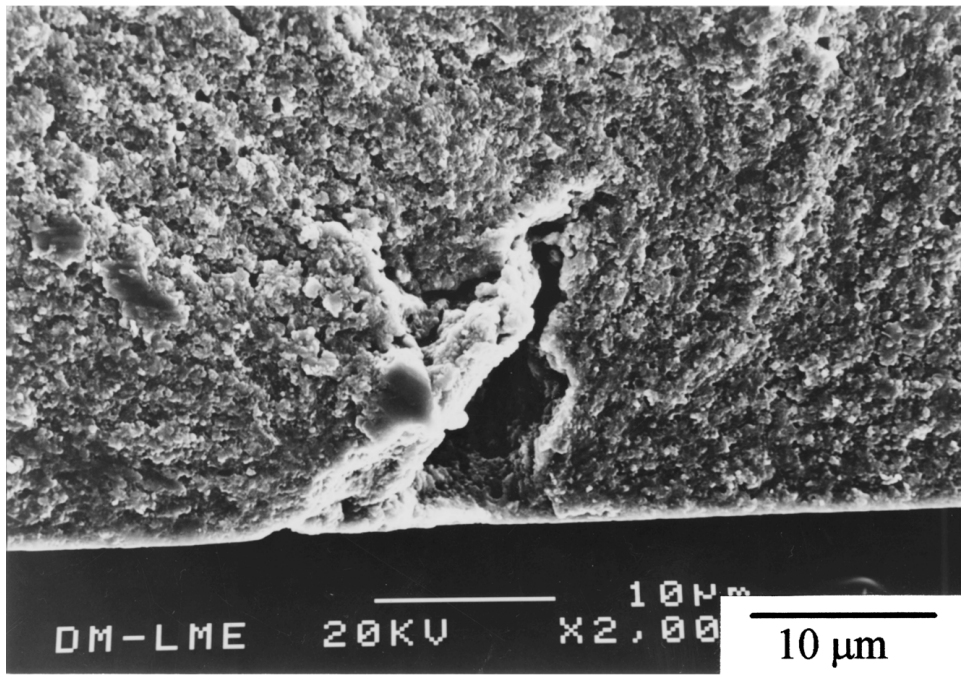

(b)

Figure 9 Failure origin in a bending bar in the as-sintered state. (a) Arrow marks failure initiation, (b) detail of the region marked by the arrow in (a) where a strength-controlling pore is surrounded by a "white-contrast" (intergranular) region.

This simplifies the fracture model because the assessment of crack growth with a preformed transformation zone would depend on the loading sequence that was applied during the early growth of the crack (i.e., crack loading history). Present assumptions are consistent with the hypothesis of crack nucleation processes which are induced by thermal mismatch upon cooling from sintering temperature (see Section 3.1). As such crack nucleation is assumed to occur at elevated temperatures where transformation toughening is not active, a transformation zone would not be present around the cracks. (It is emphasized, however, that since the R-curve of the Y-TZP under study is relatively steep during the first few microns of crack growth, the intersection between K_a and K_r would not be significantly affected in the event that a transformation zone is fully developed prior to the application of external loads. Thus, computations with a preformed transformation zone, where in the limiting case the fracture resistance of the material is assumed to be identical to the maximum toughness of

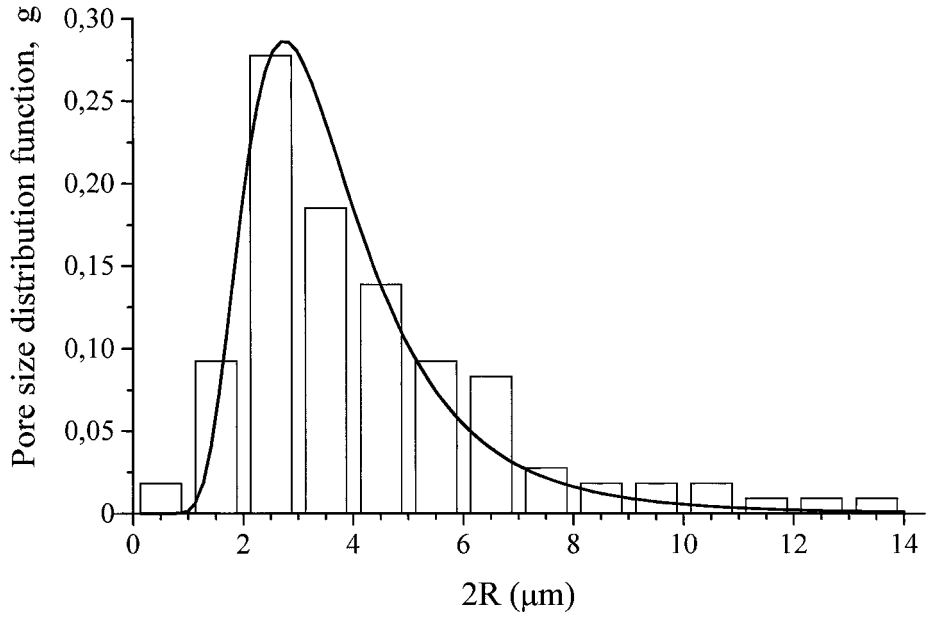

Figure 10 Distribution function, g(R), for the as-sintered Y-TZP.

the R-curve, would only shift the fracture strength distribution to higher stresses by a factor of less than 10%.)

The derivations presented in the Appendix enable the calculation of the failure probability for a given pore size distribution function, $g(R)$. As indicated in the aforementioned assumptions, the tangency condition ($K_a = K_r$) yields the fracture strength for any given pore size in $g(R)$ once the value of the normalized crack length, c/R, is known. Thus, in order to compute the fracture strength distribution in the as-sintered Y-TZP, the value of c/R was calibrated by establishing from SEM observations the size and location of the pores leading to failure in three different specimens. As the fracture load was recorded for each of the specimens, it becomes possible to compute the actual stress level at which each of the pores was subjected, and to estimate the effective value of c so that fracture is triggered when K_a intercepts the R-curve of the material, K_r. By fitting the R-curve to Equation 1, such calculation leads to initial crack lengths, c, between 0.9 and 1 μm for the three pores under examination.

From the pore size distribution function for the as-sintered Y-TZP in Fig. 10 and by taking $c = 0.95$ μm,

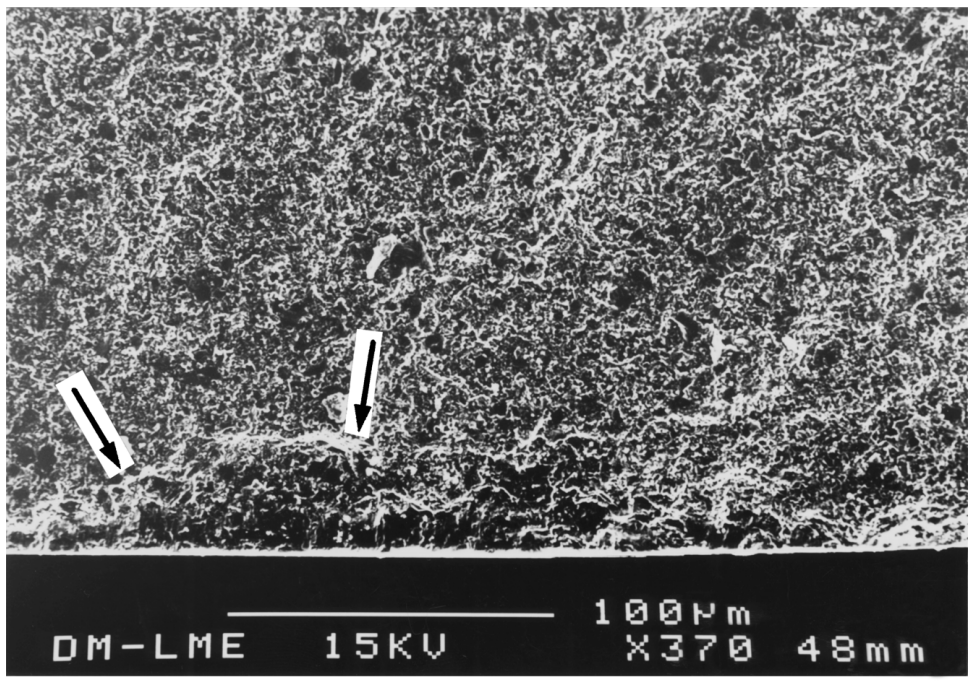

(a)

Figure 11 Failure origins in heat-treated specimens. (a) Arrows delimit failure origin. (b) Detail of the region marked in (a). (c) Clusters of cubic grains triggering failure in a different specimen *(Continued.)*

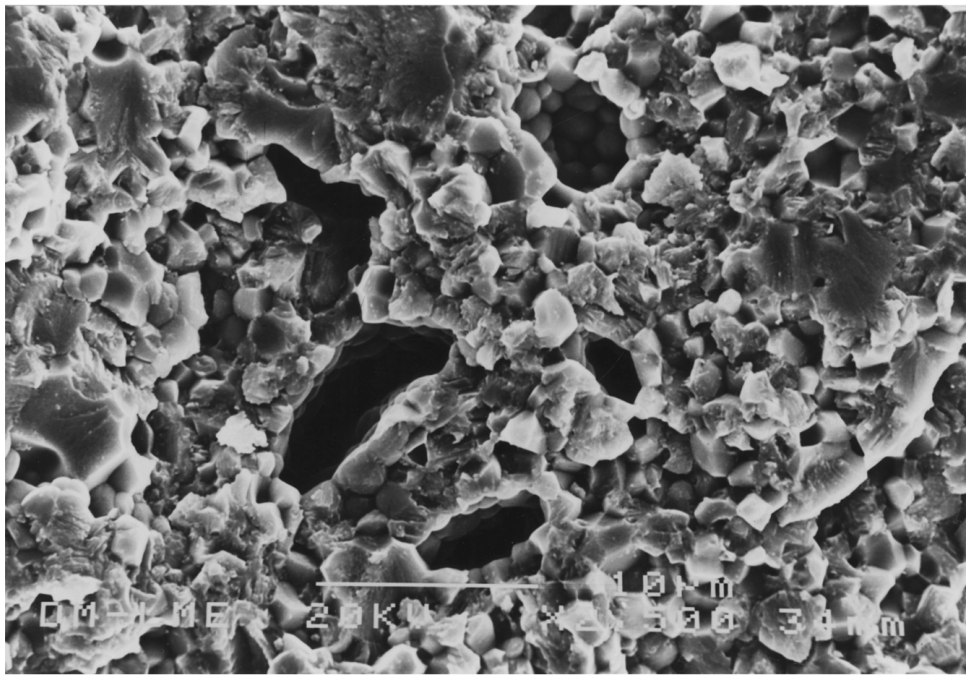

(b)

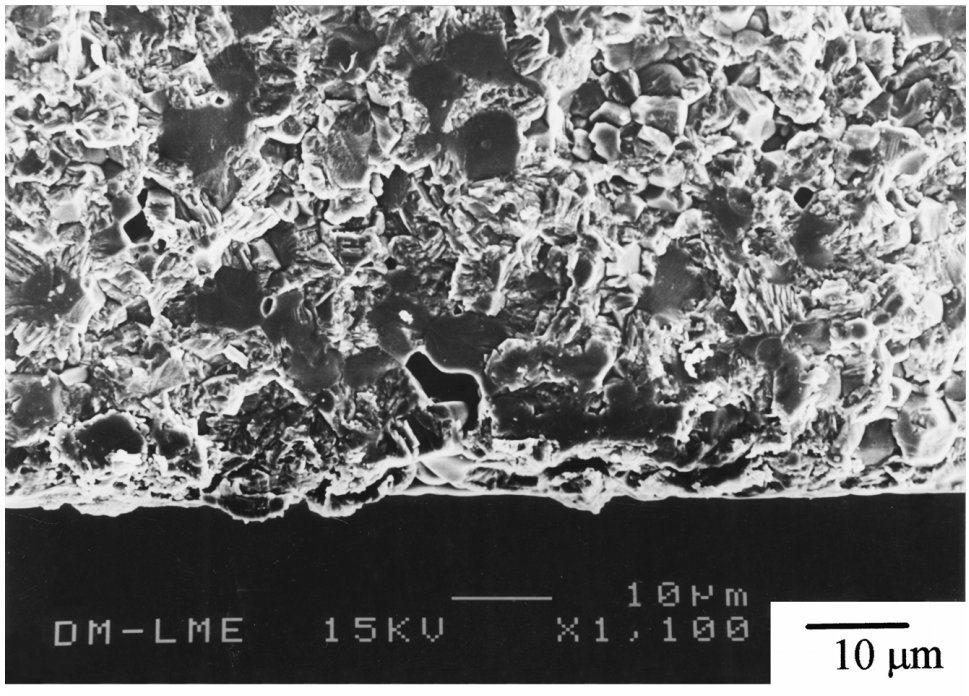

(c)

Figure 11 (Continued).

the fracture stress distribution can be computed for a unit volume of material ($V/V_o = 1$), see Fig. 6. This computation is performed by estimating the failure probability for each pore in the distribution (by numerical integration of Equation (A5)) and its associated failure stress so that $K_a = K_r$. Thus, a value of $m = 13.5$ is found by plotting the computed failure strength distribution in terms of Weibull statistics (Fig. 6).

It is found that the estimated value of m for the as-sintered Y-TZP is quite similar to that measured experimentally (see Table III). It is noticed that in such estimation, the influence of c/R on m is relatively mild as the normalized crack length mostly affects the scaling strength, σ_o, of the distribution. Obviously, present model does not allow to perform a computation of σ_o as this factor depends on the volume of material which is subjected to tensile loads (V/V_o). Thus, σ_o varies depending on the specimen size, its shape and loading conditions (bending, tensile, and the like). In this sense, it is emphasized that if the volume of the hypothetic specimens containing a representative number of pores, V_o, was taken so that $V/V_o = 150$ (see the Appendix), the computed fracture distribution would match that measured experimentally under three-point bending conditions. Such value of V/V_o confirms the observations in Ref. [21] where, by using a similar fracture

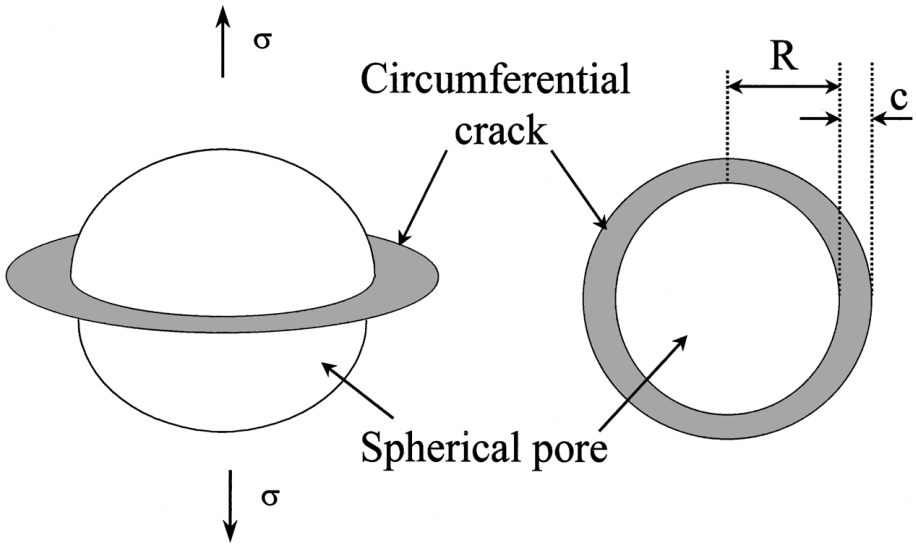

Figure 12 Schematic of a pore surrounded by a circumferential crack and the associated nomenclature.

model, it is indicated that V_o may be 100 to 1000 times smaller than that of actual bending specimens.

The value of V/V_o is anticipated to depend on the average distance between neighboring pores. An increase in such average separation implies that V_o would also have to increase in order to accommodate a sufficiently large number of pores (so that their distribution becomes representative of that present in a large volume V). The fact that $V/V_o = 150$ for the bending bars implies that as fracture is effectively triggered in a *minute* region close the free surface of the bar, V_o should be a considerably small quantity.

Within the framework of Weibull statistics, the derivations in Ref. [22] enable quantification of the decrease in fracture strength which is anticipated if the experiments were conducted under uniaxial loads rather than under three-point bending. (Such decrease in fracture strength is the result of the larger volume of material which is placed under tensile loads in the case of uniaxial loading as compared to three-point bending conditions.) In accordance to Weibull statistics, uniaxial loading conditions would shift the entire experimentally measured failure statistics to lower stresses by a factor of 0.6 while m remains constant [23]. The only means to find correspondence between the above computations for a unit volume of material and such fracture strength distribution under uniaxial loads would be to have pore sizes which are much larger that those usually encountered in polished samples (which imply the consideration of V/V_o in the order of 10^5).

4. Summary

The heat treatment of a fully tetragonal zirconia (Y-TZP) to coarsen its grain size confirms the results of prior work as grains of up to $\sim$4 μm are found to preserve their original tetragonal structure upon cooling to room temperature [5]. The increased capacity of heat-treated (Y-TZP/PSZ) materials containing such tetragonal grains to undergo a stress-assisted tetragonal-to-monoclinic (t–m) phase transformation is evidenced by an increase in the amount of monoclinic phase at the fracture surface and the development of a more pronounced R-curve behavior. Present results suggest the existence of a critical grain size above which transgranular fracture of tetragonal grains is followed by their t–m transformation. Below such critical size, t–m transformation is not attained even when the tetragonal grains may fracture in a transgranular fashion. The latter is the case of the as-sintered Y-TZP studied in this work.

Present results show that failure origins are influenced by microstructural coarsening. In the case of the as-sintered Y-TZP with finer grains, failure originates by pores whose average size is of $\sim$10 μm. Therefore, a reduction of pore size is expected to bring about an increase in the fracture strength of this material. As the grain size coarsens leading to materials with a mixed Y-TZP/PSZ character, failure is not longer triggered by single pores but by larger defects whose size ranges from 30–60 μm. These defects seem to be induced by t–m transformation which leads to microcrack coalescence around multiple pores. Alternatively, failure origins in the heat-treated materials may also involve clusters of cubic grains. From the point of view of the relationship between the R-curve and fracture strength, simple fracture mechanics estimations indicate that the increase in the size of the critical defect in the heat-treated Y-TZP/PSZ materials is compensated by a rise in their fracture toughness. Consequently, fracture strength distributions in Y-TZP/PSZs are similar to those in the as-sintered Y-TZP.

A simplified fracture model is used to compute the fracture strength distribution in the small grained Y-TZP from a knowledge of its R-curve behavior and pore size distribution. It is found that the material constant m which dictates the fracture variability according to Weibull statistics can be computed from such fracture model as its value is similar to that measured experimentally. The scaling strength σ_o of the Weibull statistics depends on the volume of material which is subjected to tensile loading. Thus, its computation from the fracture model is not direct and requires experimental calibration.

Acknowledgments

The authors are grateful to M. Marsal for experimental assistance on the SEM and to A. Campillo for arranging the supply of the Y-TZP bars. This work was supported by Generalitat de Calalunya under grant 1999SGR00129 and CICYT under grant MAT97-0923. The first author acknowledges Generalitat de Catalunya for supporting his PhD work through a FI scholarship.

Appendix

Consider a unit volume of material, V_o, subjected to tensile loads with a representative pore size distribution. In the assumption that fracture is induced by the largest pore present in the material, the failure probability is given by

$$P_f = \int_{R_i}^{\infty} g(R)\,\mathrm{d}R, \tag{A1}$$

where $g(R)$ is the distribution function which gives the probability that any given pore size, R_i, is present in V_o. In Equation A1, $g(R)$ is taken so that when integrated between 0 and ∞, $P_f \equiv 1$. Being this the case, the survival probability, P_s, $= (1 - P_f)$ is given by

$$P_s = 1 - \int_{R_i}^{\infty} g(R)\,\mathrm{d}R \tag{A2}$$

The survival probability of a generic volume of material (V), where $V = nV_o$, is then equal to P_s^n. Consequently,

$$P_s\big|_V = \left(1 - \int_{R_i}^{\infty} g(R)\,\mathrm{d}R\right)^{V/V_o}. \tag{A3}$$

By noting that for any number κ, $(1 - \frac{\kappa}{V/V_o})^{V/V_o} \sim e^{-\kappa}$ when $V \gg V_o$, it follows that Equation A3 can be written as

$$P_s\big|_V = \exp\left(-\frac{V}{V_o}\int_{R_i}^{\infty} g(R)\,\mathrm{d}R\right). \tag{A4}$$

Thus, the failure probability of a generic volume of material, V, is given by

$$P_f\big|_V = 1 - \exp\left(-\frac{V}{V_o}\int_{R_i}^{\infty} g(R)\,\mathrm{d}R\right) \tag{A5}$$

References

1. B. LAWN, "Fracture of Brittle Solids," 2nd ed. (Cambridge University Press, 1993).
2. R. W. RICE, *J. Mater. Sci.* **32** (1997) 1673.
3. D. B. MARSHALL, *J. Amer. Ceram. Soc.* **69** (1986) 173.
4. M. V. SWAIN and L. R. F. ROSE, *ibid.* **69** (1986) 511.
5. L. RUIZ and M. J. READEY, *ibid.* **79** (1996) 2331.
6. F. L. CUMBRERA, F. SÁNCHEZ-BAJO, R. FERNÁNDEZ and L. LLANES, *J. Eur. Ceram. Soc.* **18** (1998) 2247.
7. D. R. CLARKE and F. ADAR, *J. Amer. Ceram. Soc.* **65** (1982) 284.
8. M. S. KALISZEWSKI, G. BEHRENS, A. H. HEUER, M. C. SHAW, D. B. MARSHALL, G. W. DRANSMANN, R. W. STEINBRECH, A. PAJARES, F. GUIBERTEAU, F. L. CUMBRERA and A. DOMIN-GUEZ, *ibid.* **77** (1994) 1185.
9. R. F. COOK, L. M. BRAUN and W. R. CANNON, *J. Mater. Sci.* **29** (1994) 2133.
10. J. ALCALÁ and M. ANGLADA, *Mater. Sci. Eng.* **A245** (1998) 267.
11. G. QUINN, J. KÜBLER and R. GETTING, VAMAS Report # 17, NIST, Gaithersburg MD, USA (1993).
12. R. F. COOK and B. R. LAWN, *J. Amer. Ceram. Soc.* **66** (1983) C–200.
13. J. C. NEWMAN and I. S. RAJU, *Engng. Fract. Mech.* **15** (1981) 185.
14. A. G. EVANS, "Advances in Ceramics: Science and Technology of Zirconia II," edited by N. Claussen, M. Rühle and A. H. Heuer (Am. Ceram. Soc., Ohio, USA, 1980) p. 193.
15. R. K. GOVILA, *J. Mater. Sci.* **30** (1995) 2656.
16. J. ALCALÁ and M. ANGLADA, *Mater. Sci. Eng.* **A232** (1997) 103.
17. A. ZIMMERMANN, M. HOFFMAN, B. D. FLINN, R. K. BORDIA, T.-J. CHUANG, E. R. FULLER and J. RÖDEL, *J. Amer. Ceram. Soc.* **81** (1998) 2449.
18. R. W. RICE, *J. Mater. Sci.* **19** (1984) 895.
19. F. I. BARATTA, *J. Amer. Ceram. Soc.* **64** (1981) C–3.
20. T. FETT, *Int. J. Fract.* **67** (1994) R–41.
21. R. DANZER and T. LUBE, in "Fracture Mechanics of Ceramics 11," edited by Bradt *et al.* (Plenum Press, NY, USA, 1996) p. 425.
22. P. STANLEY, H. FESSLER and A. D. SIVILL, *Proc. Brit. Ceram. Soc.* **22** (1973) 453.
23. *Idem.*, *Proc. Inst. Mech. Engrs.* **190** (1976) 589.

Received 15 March
and accepted 27 November 2000